Excitations of Multiple Fano Resonances Based on Permittivity-Asymmetric Dielectric Meta-Surfaces for Nano-Sensors

Yusen Wang, Shilin Yu, Ziang Gao, Shaozhe Song, Hongyun Li, Tonggang Zhao, and Zonghai Hu

***Abstract*—We have designed an all-dielectric device based on permittivity-asymmetric rectangular blocks on meta-surfaces, yielding multiple Fano resonances with high sensitivity and high figure of merit (FOM) in the near-infrared regime. By introducing different materials to break the permittivity-symmetry, three sharp Fano peaks are generated with high Q-factors arising from the interference between the sub-radiant modes and the magnetic dipole resonance modes. Combining the field distributions and the multipole decomposition in Cartesian coordinates, the resonance modes are analyzed to be magnetic quadrupoles (MQs) and magnetic dipoles (MDs). Furthermore, the dependence on materials and geometric parameters has been studied. The maximal sensitivity, FOM and Q-factor reach 394 nm/RIU, 4925 and 14437, respectively. This proposed structure provides a good alternative to geometry-asymmetric meta-surface structures and may be used for multichannel sensing, nonlinear optical devices, and laser.**

***Index Terms*—Permittivity-asymmetry, BIC, high sensitivity, meta-surface, Fano resonance, nano-sensor.**

I. Introduction

HIGH sensitivity sensors play a significant role in the field of opto-electronic applications, such as lasers [1], nonlinear optics [2], and optical switching [3]. To enhance device performance, High Q-factor resonances have been widely employed, including Fano resonance and bound states in the continuum (BIC) [4]–[8]. Fano resonance is a phenomenon manifested as an asymmetric spectral feature (Fano shape) due to the interference of a narrow resonance with a much broader band of states (continuum). BICs are localized waves coexisting with a continuous spectrum of radiating waves due to destructive interference in which the coupling with all radiative waves vanish. In practice, BIC can be realized as a quasi-BIC mode when both the Q factor and the resonance width become finite in a Lorentzian shape. A close link between BICs and Fano resonances was revealed recently on meta-surfaces [21], the transmission spectra of dielectric meta-surfaces can be described explicitly by the classical Fano formula near the conditions for the quasi-BIC.

Javier Gonzalez-Colsa [9] designed a tunable grating-based high sensitivity plasmonic sensor using metal materials, and the sensitivity was up to 1500 nm/RIU. However, the Q-factor of the metal-based structure was low [10], which had more Ohmic losses. In opto-electronic systems, most of the devices are made of commonly used semiconductor materials [11], [12], such as Silicon (Si), Germanium (Ge), gallium arsenide (GaAs), and indium arsenide (InAs) etc. [13]. Therefore, studying and realizing high sensitivity resonances in these commonly used semiconductor materials is important [14]–[16]. Recently, high sensitivity dielectric meta-surfaces are developed [17]. Dielectric meta-surfaces can support both electric and magnetic dipolar Mie-type resonances [18] and avoid the Ohmic losses efficiently, generating much narrower Fano resonances compared with traditional plasmonic meta-surfaces [19]. They can also excite strong magnetic and toroidal responses [20]. In dielectric meta-surfaces, electric and magnetic dipole oscillations would be generated when the incident plane wave has an electric field polarization along a specific direction of a symmetric structure [21]. The wide spectral line thus formed can be seen as a bright mode (radiative band). Breaking the in plane inversion symmetry can change the distribution of the dipole moments, causing the different displacement current [22] and a quasi-BIC. As a result, near-field coupling would restrain the energy of radiation, which can be seen as a dark mode (localized state). When the coupling of the bright mode and the dark mode occurs in the vicinity of quasi-BIC, sharply asymmetric Fano resonances would be excited [23]. Multipole decomposition is an effective method to analyze different multipole contributions on excited electromagnetic resonances [24], such as electric dipole (ED), magnetic dipole (MD), electric quadrupole (EQ), magnetic quadrupole (MQ), and toroidal dipole (TD). Combining the results of multipole decomposition and the field distribution, the origin of Fano resonances can be analyzed.

Due to demand in multichannel devices, recent research in optical Fano resonances has extended from single Fano resonance to multiple Fano resonances. Gui-Dong Liu *et al.* [25]

Manuscript received December 6, 2021; revised January 9, 2022; accepted January 16, 2022. Date of publication January 21, 2022; date of current version February 4, 2022. This work was supported in part by the National Key R&D Program of China under Grants 2018YFB2200402, 2017YFB0403602, and 2016YFB0400603, and in part by the National Natural Science Foundation of China under Grant 61835002. *(Corresponding authors: Hongyun Li; Tonggang Zhao; Zonghai Hu.)*

Yusen Wang, Shilin Yu, Ziang Gao, Shaozhe Song, Tonggang Zhao, and Zonghai Hu are with the School of Electronic Engineering, Beijing University of Posts and Telecommunications, Beijing 100876, China (e-mail: wangyusen@bupt.edu.cn; yushilin@bupt.edu.cn; zagao@bupt.edu.cn; songsz2019@bupt.edu.cn; zhaotg@bupt.edu.cn; zhhu@bupt.edu.cn).

Hongyun Li is with the State Key Laboratory for Artificial Microstructure and Mesoscopic Physics, School of Physics, Peking University, Beijing 100871, China (e-mail: lihongyun@pku.edu.cn).

Digital Object Identifier 10.1109/JPHOT.2022.3144399

This work is licensed under a Creative Commons Attribution 4.0 License. For more information, see https://creativecommons.org/licenses/by/4.0/

proposed a refractive index sensor based on Fano resonance in Si split-ring meta-surface with a sensitivity of 452 nm/RIU and a figure of merit of 56.5. Xu Chen *et al.* [26] proposed a terahertz sensor of which the sensitivity is 1.96GHz/RIU and the FOM is up to 3189. One simulation of a sensor with Fano-resonances and polarization-insensitivity was reported by Liu *et al.* [27] with a sensitivity of 186.96 nm/RIU and FOM of 721. However, experimental results are scarce due to fabrication difficulty.

One important way to generate Fano resonances is symmetry breaking. The most widely used method is by geometrical symmetry breaking. However, this method requires high accuracy of fabrication to achieve high Q-factor and high sensitivity. Katie E. Chong *et al.* [28] demonstrated a functional silicon meta-device to control the wavefront of optical beams. Alternatively, using different materials in different parts of the structure can generate permittivity asymmetry. This method can lower the requirement on spatial resolution. Xingguang Liu *et al.* [29] reported a permittivity-asymmetric dielectric meta-surface with dual-toroidal dipole excitation on it, which indicates the multipole resonances can be excited in the permittivity-asymmetry system. More work on generating Fano resonances and achieving high sensitivity through the permittivity-asymmetry is still needed.

In this work, by using different materials to generate permittivity-asymmetry, three sharp Fano peaks arising from the interference between the sub-radiant modes and the dipole resonance modes are generated. Combining the field distribution and the multipole decomposition in Cartesian coordinates, different resonance modes at the Fano peaks are analyzed numerically. After choosing appropriate materials and geometric parameters, the maximal FOM reaches 4925, the highest among published meta-surface structures. This study provides a new possibility for high sensitivity nano sensors.

II. Structure Design

The structure is designed as periodical symmetric rectangular blocks. As shown in Fig. 1(a), there are three cells in the x-direction and four cells in the y-direction. Different colors of the substrate and the rectangular blocks represent different materials of different parts. The unit cell is composed of two blocks with the same shape on silicon substrate. Permittivity asymmetry is formed by using two different materials for the two blocks. Numerical simulations are based on the finite-difference time-domain (FDTD) method. In numerical simulation, the incident wave is set as plane wave with the polarization along the y-axis.

III. Simulation Results and Discussions

Fig. 2(a) shows the transmission spectra of the dielectric meta-surface. The geometrical parameters are set as shown in Fig. 1(a) and (b): Px = 725 nm, Py = 530 nm, t = 500 nm, L = 280 nm, w = 200 nm, and d = 75 nm. And the related simulation is set with mesh grid density level7, periodic boundary conditions in x and y directions and the auto cutoff at 1E-5. When both blocks of the unit cell are Si blocks, the corresponding transmission

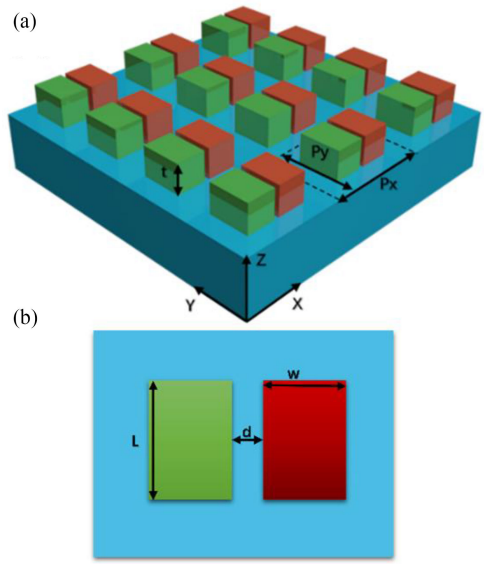

Fig. 1. (a) Schematic of the permittivity-asymmetric dielectric meta-surface on silica substrate. (b) Top view and geometric parameters of the cell. Px = 725 nm, Py = 530 nm, t = 500 nm, L = 280 nm, w = 200 nm, and d = 75 nm.

spectrum is shown by the dotted curve. When the left block is silicon and the right block is InAs, the permittivity-asymmetry is formed and the corresponding transmission is shown by the red curve. Three asymmetric Fano peaks are observed around the wavelength of 1067.2 nm, 1183.6 nm, and 1214.7 nm. Previously in geometric asymmetric structures, the asymmetry degree is defined by geometric parameters, such as the slightly different widths of two Si bars used in Yuebian Zhang's work [30]. Here we define the asymmetry degree (δ) as $= \Delta n/n$, in which n is the refractive index of materials, and Δn is the variance of n.

Evolution of the modes is shown in Fig. 2(d). When the asymmetry degree $\delta = 0$, one resonance mode F due to the structure array of the meta-surface is observed. With the increase of δ, three additional asymmetric resonance modes appear due to breaking the in-plane symmetry. The slight redshift is due to the change of the effective refractive index. As shown in Fig. 2(c), the radiative Q-factor satisfies the inversely proportional relation with δ^2 relatively well, strongly indicating that the structure parameters are near the quasi-BIC conditions and the observed Fano resonances are quasi-BIC linked [21], [31].

The multipole decomposition in Cartesian coordinates is calculated and shown in Fig. 3. The formula of each dipole moment is given [32] in Table I.

Five basic different modes of electro-magnetic resonances have been generated at the three transmission peaks. There are two kinds of dominant resonance modes, MQ and MD. At 1067.2 nm and 1183.6 nm, MQ is the dominant resonance mode. At 1214.7 nm, MD is the dominant resonance mode. As of the resonance at 1160.4 nm not due to permittivity-asymmetry, TD is the dominant resonance mode.

The electric and magnetic field distributions are shown in Fig. 4. The left block is Si and the right block is InAs. At 1067.2 nm. Four magnetic currents generated by ring electric

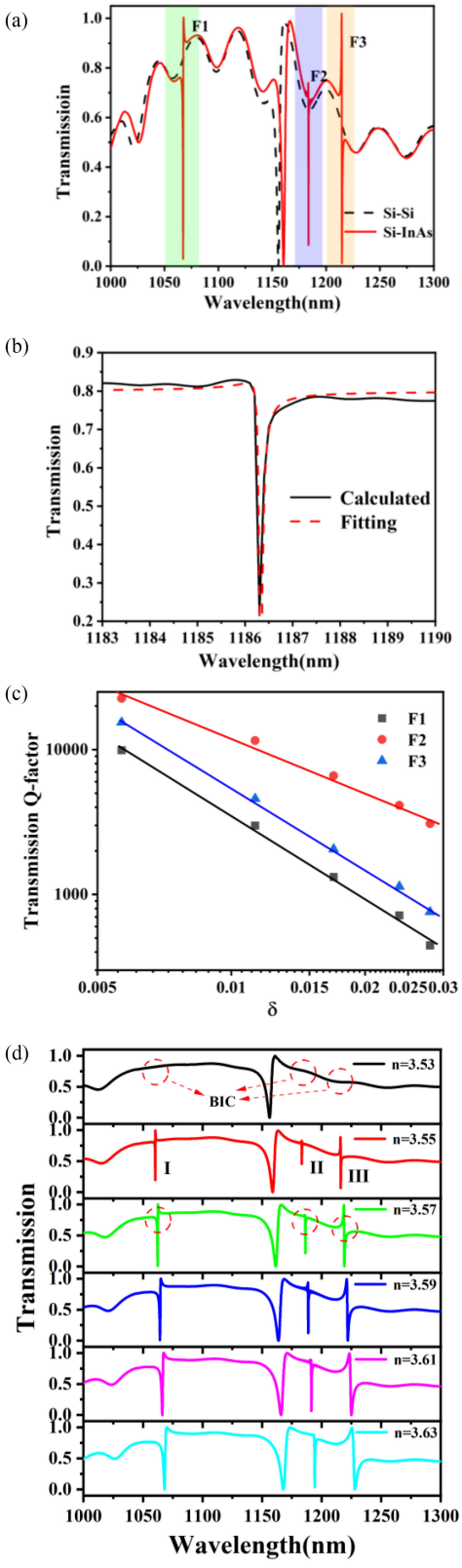

Fig. 2. (a) Transmission spectra of the meta-surface with permittivity symmetry and asymmetry. (b) The fitted spectrum near the F2 resonance according to the classical Fano formula, and the calculated spectrum by FDTD method. (c) The relation between the Q-factor and δ^2. (d) Simulation results with the refractive index n of the right block ranging from 3.53 to 3.63.

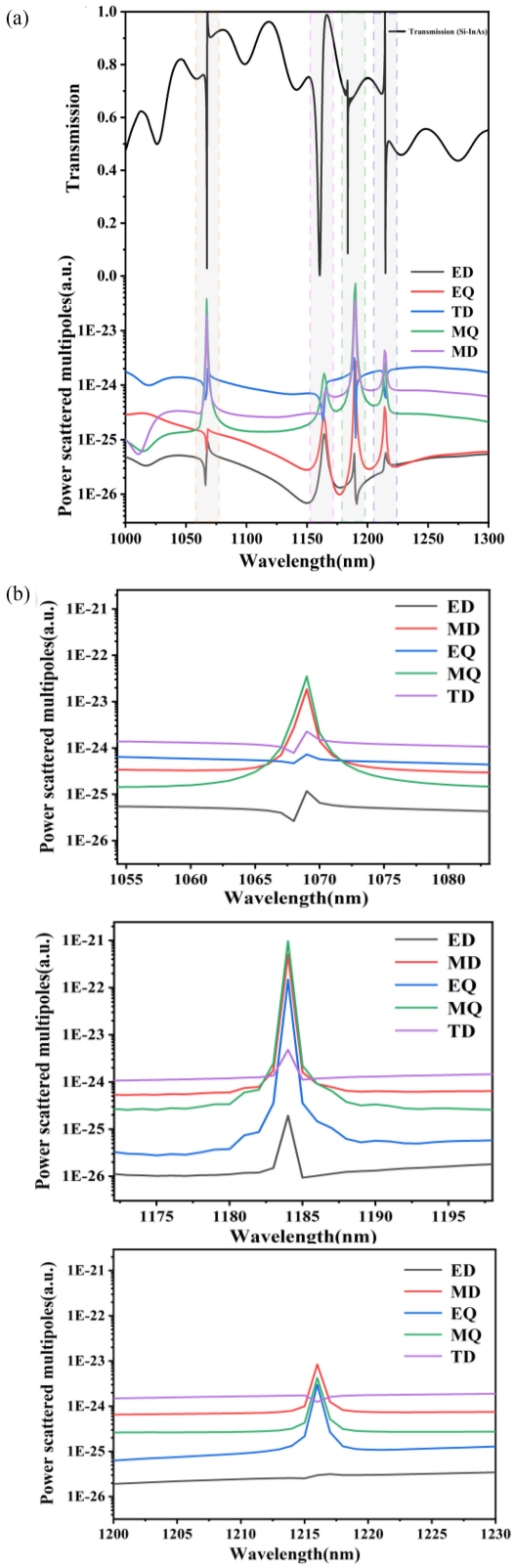

Fig. 3. (a) Contributions of resonance modes. (b) Details of multipole contributions at the three Fano peaks.

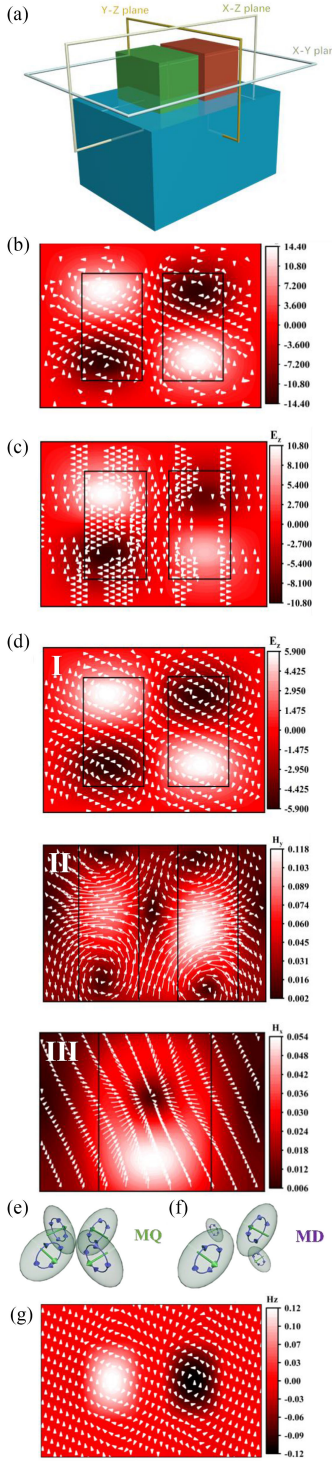

Fig. 4. Field distributions at the three Fano peaks. (a) The schematic plane diagram. (b) Field distribution in the x-y plane at 1067.2 nm. (c) Field distribution in the x-y plane at 1183.6 nm. (d-I) Field distribution in the x-y plane at 1214.7 nm. (d-II) Magnetic field distribution in the x-z plane at 1214.7 nm. (d-III) Magnetic field distribution in the y-z plane at 1214.7 nm. (e) Schematic of the MQ resonance. (f) Schematic of the MD resonance. In (b), (c), and (d-I), the color scales represent the amplitude of the out-of-plane component of the electric field, the white vectors indicate the in-plane component distribution of the magnetic field. In (d-II) and (d-III), the color scales represent the amplitude of the out-of-plane component of the magnetic field, the white vectors indicate the in-plane component distribution of the magnetic field. (g) Magnetic field distribution in the y-z plane at 1160.4 nm.

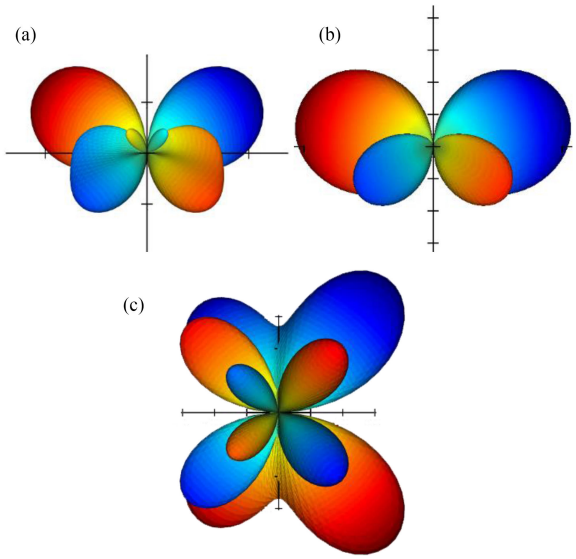

Fig. 5. The simulation results of far field radiation at 1067.2 nm, 1183.6 nm, and 1214.7 nm.

currents are observed in the x-y plane. The magnetic field in the two blocks along the y-z and x-z planes can be obtained by the right-hand-rule from the electric field distribution shown in Fig. 4(b). According to the analysis above, the magnetic fields in the two blocks are in opposite directions along the x axis. Meanwhile, the electric field in the y-z plane forms two reversed current loops. The above field features point to an MQ resonance. Similarly, the field distribution at 1183.6 nm show in Fig. 4(c) also indicates an MQ mode. As shown in Fig. 4(d) for the 1214.7 nm resonance, there are two magnetic currents rotating in opposite directions in the y-z and x-z planes. However, the amplitude of the magnetic current in the y-z plane is nearly twice as the one in the x-z plane. This can be explained by stronger MD mode in the y-z plane as illustrated in Fig. 4(f). Consistent with the field distribution results, the amplitude of the MD resonance is about twice the MQ resonance. Fig. 4(e) and (f) are schematic diagrams of the MQ and MD resonances. An MQ resonance has four current loops with the same amplitude. The MD resonance at 1214.7 nm also has four loops, however two of them are much smaller.

Simulation of far field radiation is shown in Fig. 5. It is also consistent with the above mode analysis results.

Several semiconductor materials have been chosen to find the appropriate permittivity-asymmetry for optimal performance. The left block material is Si. InAs, GaAs, InP, and Ge have been chosen to be the material of the right block, effectively varying the asymmetry parameter δ. The resulting transmission spectra are shown in Fig. 6. For InP and Ge, the Fano peaks disappear because the permittivity-asymmetry is too large to have a significant Q. For GaAs, a similar spectrum to that of InAs is observed, the main resonance modes forming the Fano peaks are MQ, MQ, and MD at wavelength of 1054.6 nm, 1172.4 nm, and 1198.7 nm, respectively.

Geometric parameters L and w have also been varied. w has been varied from 180 nm to 220 nm. L has been varied from

TABLE I
FORMULA OF EACH DIPOLE MOMENTS IN CARTESIAN COORDINATES

Order	Dipole moments	Far-field scattering intensities
1. electric dipole	$\vec{P} = \frac{1}{i\omega}\int \vec{j} d^3r$	$I_P = \frac{2\omega^4}{3c^3}\left\|\vec{P}\right\|^2$
2. magnetic dipole	$\vec{M} = \frac{1}{2c}\int \vec{r} \times \vec{j} d^3r$	$I_M = \frac{2\omega^4}{3c^3}\left\|\vec{M}\right\|^2$
3. toroidal dipole	$\vec{T} = \frac{1}{10c}\int [(\vec{r}\cdot\vec{j})\vec{r} - 2r^2\vec{j}] d^3r$	$I_T = \frac{2\omega^6}{3c^5}\left\|\vec{T}\right\|^2$
4. electric quadrupole	$Q^e_{\alpha\beta} = \frac{1}{i2\omega}\int [r_\alpha j_\beta + j_\beta r_\alpha - \frac{2}{3}(\vec{r}\cdot\vec{j})] d^3r$	$I_{Q^{(e)}} = \frac{\omega^6}{5c^5}\sum\left\|\vec{Q}^{(e)}_{\alpha,\beta}\right\|^2$
5. magnetic quadrupole	$Q^m_{\alpha\beta} = \frac{1}{3c}\int [(\vec{r}\times\vec{j})_\alpha r_\beta + ((\vec{r}\times\vec{j})_\beta r_\alpha)] d^3r$	$I_{Q^{(m)}} = \frac{\omega^6}{40c^5}\sum\left\|\vec{Q}^{(m)}_{\alpha,\beta}\right\|^2$

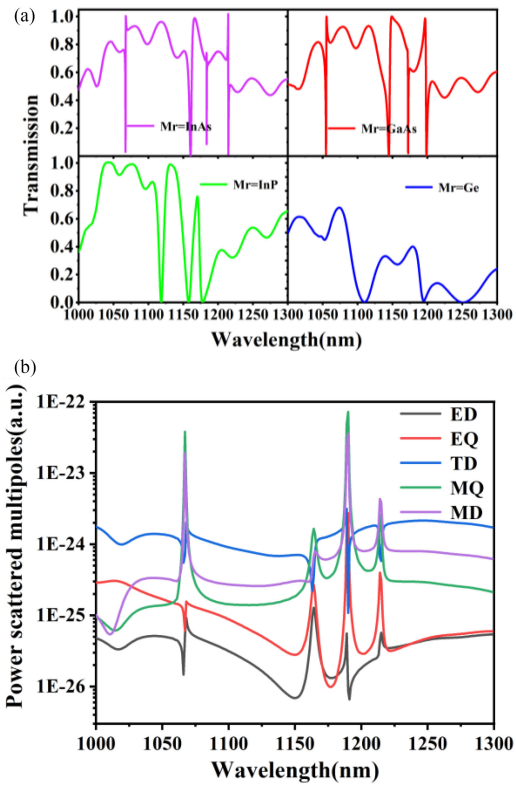

Fig. 6. (a) Transmission spectra of the structure with different materials. (b) Contributions of multipoles for the GaAs structure.

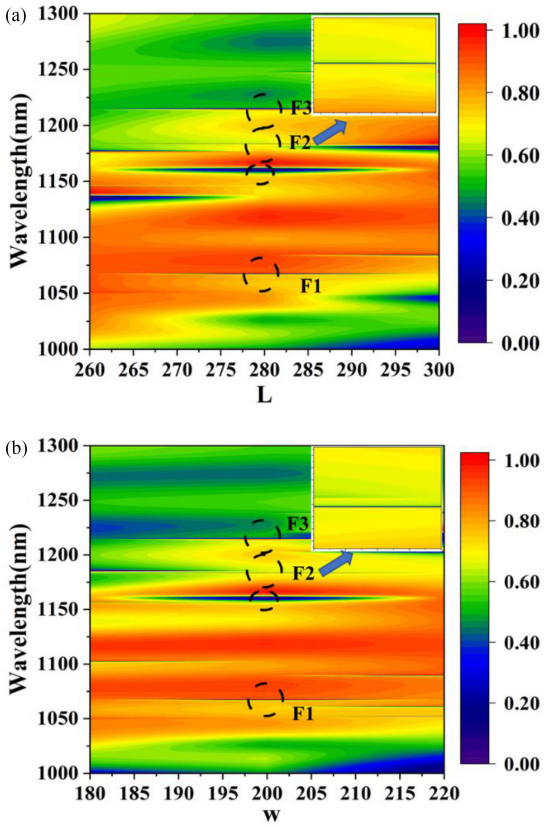

Fig. 7. Transmission spectra of the structure with different geometric parameters. (a) Evolution of transmission spectra varying L. (b) Evolution of transmission spectra varying w. The color scale represents the intensity of transmission. Insets: Enlarged views of the F2 circled areas.

260 nm to 300 nm. The color scale in Fig. 7 represents the intensity of transmission. Fano peaks at 1067.2 nm, 1183.6 nm, and 1214.7 nm can be identified in the figures. Sharpest Fano peaks are resulting from L = 280 nm and w = 200 nm.

In application, this structure can be used as a refractive index sensor with high sensitivity. Fig. 8(a) shows the transmission spectra of the permittivity-asymmetric structure with silicon substrate and the refractive index n hypothetically ranging from 1.00 to 1.10. As in optical resonant sensors, the performance is generally described by the full width at half maxima $\Delta\lambda$. The sensitivity of meta-surfaces can be defined as

$$S = [\lambda(n2) - \lambda(n1)]/(n2 - n1) \quad (1)$$

in which n1 and n2 are the background refractive indices [33]. For better description of the sensing properties, combining these two features, the figure of merit (FOM) is introduced as $S/\Delta\lambda$. High sensitivity, FOM and Q-factor are desirable in devices [34]. Calculated from Fig. 8, the sensitivities of the three Fano peaks

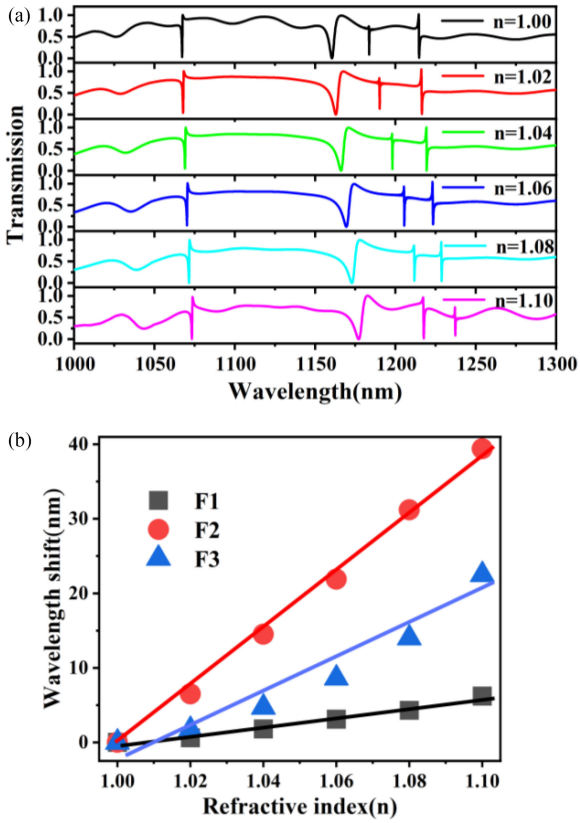

Fig. 8. (a) Transmission spectra with refractive indices of 1.00, 1.02, 1.04, 1.06, 1.08, and 1.10. (b) The red shift of the center wavelengths of the Fano peaks versus the refractive index.

around 1067.2 nm, 1183.6 nm and 1214.7 nm are 62 nm/RIU, 394 nm/RIU, 225 nm/RIU, respectively. The FOM of the peaks are 155, 4825, and 125, respectively. The center wavelengths of the Fano peaks undergo an almost linear redshift with increase of n, as shown in Fig. 8(b). This linear relation is beneficial to a sensor. The fitted curves in Fig. 9 are calculated by the classical Fano formula

$$T(\omega) = T_0 + A_0 \frac{[q + 2(\omega - \omega_0)/\tau]^2}{1 + [2(\omega - \omega_0)/\tau]^2} \tag{2}$$

where ω_0 is the resonant frequency, τ is the resonance linewidth, T_0 is the transmission offset, A_0 is the continuum-discrete coupling constant, and q is the Brit-Wigner-Fano parameter. According to the classical Fano formula, Fano line shape in meta-surfaces can be given as

$$T_{Fano} = |a_1 + ia_2 + \frac{b}{\omega - \omega_0 + i\gamma}|^2 \tag{3}$$

where a_1, a_2 are constant numbers, ω_0 is the oscillation frequency, and γ is the damping factor, and the Q-factors can be calculated by $Q_{rad} = \frac{\omega_0}{2\gamma}$. The values of separate fitting parameters are given in Table II.

The Q-factors of the three Fano peaks are 1829, 14436, and 2892 respectively. The multi-modal response and the sharp Fano peaks make this structure suitable for refractive index sensing. Especially, the highest sensitivity, FOM, and Q-factor can be simultaneously achieved in the second Fano peak around the wavelength of 1214.7 nm.

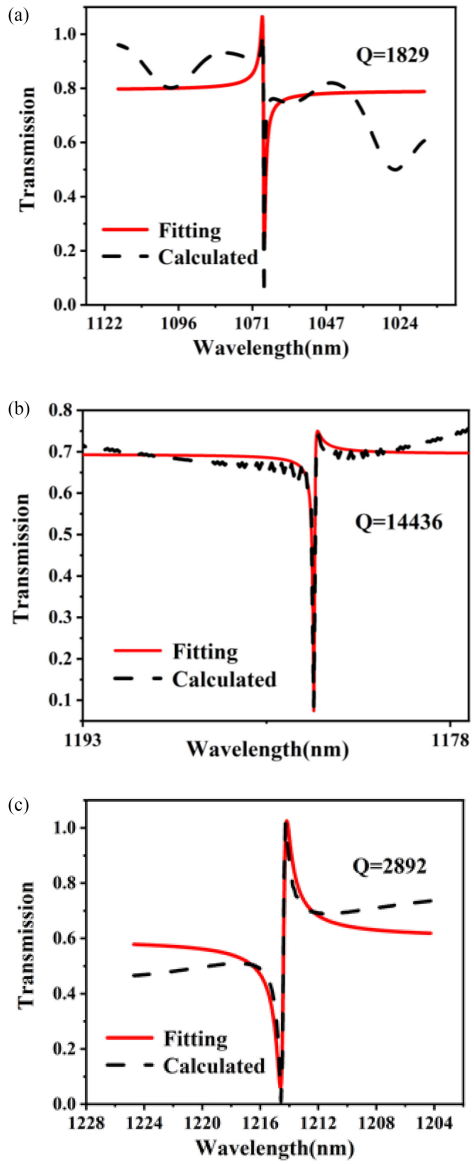

Fig. 9. The fitted spectra near the resonances and the calculated Q-factors.

TABLE II
VALUES OF SEPARATE FITTING PARAMETERS

	F1	F3	F2
a1	0.649	0.30401	0.62441
a2	0.55757	0.77581	0.45678
b	-2.7882E11	3.39842E10	2.0594E11
γ	-4.82752E11	5.51583E10	2.68297E11

Comparison with recently published meta-surface nano-sensors is shown in Table III. The permittivity-asymmetric structure proposed in this work achieves the highest FOM, showing great potential as an alternative to geometry-asymmetric structures.

TABLE III
COMPARISON WITH RECENTLY PUBLISHED META-SURFACE SENSORS

Reference	Type	FOM	Q-factor
[25]	Type-1	56.5	133
[27]	Type-1	721	5126
[35]	Type-1	99.3	170
[36]	Type-1	389	**43000**
[30]	Type-1	2846	10^5
[9]	Type-2	161.46	214.69
This work	Type-3	**4925**	14436

a. Type-1 represents Dielectric-based Metamaterial in geometry-asymmetry.
b. Type-2 represents Metal-based Metamaterial of grating-shape.
c. Type-3 represents Dielectric-based Metamaterial in permittivity-asymmetry.

IV. SUMMARY

A permittivity-asymmetric dielectric meta-surface with multiple sharp transmission Fano resonances has been designed. There are three permittivity-asymmetry generated Fano peaks. Materials and the geometric parameters have been varied to achieve the best sensitivity, FOM, and Q-factor simultaneously, reaching 394 nm/RIU, 4925 and 14436 respectively at the wavelength of 1183.6 nm with InAs for the right block and Si for the left block. Resonance modes at 1067.2 nm, 1183.6 nm, and 1214.7 nm are MQ, MQ and MD, respectively. The close-to-inversely-proportional relation between the Q-factor and the asymmetric parameter δ^2 indicates that the observed Fano resonances are quasi-BIC linked, further enriching methods to generate quasi-BICs. This permittivity-asymmetric dielectric meta-surface with multiple sharp resonances offers a good platform for multichannel sensing as well as optical modulation.

DISCLOSURES

The authors declare no conflicts of interest.

REFERENCES

[1] N. I. Zheludev, S. L. Prosvirnin, N. Papasimakis, and V. A. Fedotov, "Lasing spaser," *Nat. Photon.*, vol. 2, 2008, Art. no. 351.
[2] S.-D. Liu *et al.*, "Polarization-independent multiple fano resonances in plasmonic nonamers for multimode-matching enhanced multiband second-harmonic generation," *ACS Nano*, vol. 10, 2016, Art. no. 1442.
[3] C. Argyropoulos, "Enhanced transmission modulation based on dielectric metasurfaces loaded with graphene," *Opt. Exp.*, vol. 23, 2015, Art. no. 23787.
[4] S. Campione *et al.*, "Broken symmetry dielectric resonators for high quality factor fano metasurfaces," *ACS Photon.*, vol. 3, 2016, Art. no. 2362.
[5] C. Nicolaou, W. T. Lau, R. Gad, H. Akhavan, R. Schilling, and O. Levi, "Enhanced detection limit by dark mode perturbation in 2D photonic crystal slab refractive index sensors," *Opt. Exp.*, vol. 21, 2013, Art. no. 31698.
[6] Y. Zhong *et al.*, "Ultrasensitive specific sensor based on all-dielectric metasurfaces in the terahertz range," *RSC Adv.*, vol. 10, 2020, Art. no. 33018.
[7] A. E. Miroshnichenko, S. Flach, and Y. S. Kivshar, "Fano resonances in nanoscale structures," *Rev. Mod. Phys.*, vol. 82, 2010, Art. no. 2257.
[8] C. W. Hsu, B. Zhen, A. D. Stone, J. D. Joannopoulos, and M. Soljačić, "Bound states in the continuum," *Nat. Rev. Mater.*, vol. 1, 2016, Art. no. 16048.
[9] J. González-Colsa, G. Serrera, J. M. Saiz, F. González, F. Moreno, and P. Albella, "On the performance of a tunable grating-based high sensitivity unidirectional plasmonic sensor," *Opt. Exp.*, vol. 29, 2021, Art. no. 13733.
[10] Y. Fan *et al.*, "Achieving a high- Q response in metamaterials by manipulating the toroidal excitations," *Phys. Rev. A*, vol. 97, 2018, Art. no. 033816.
[11] I. Staude and J. Schilling, "Metamaterial-inspired silicon nanophotonics," *Nat. Photon.*, vol. 11, 2017, Art. no. 274.
[12] A. Novitsky, T. Repän, R. Malureanu, O. Takayama, E. Shkondin, and A. V. Lavrinenko, "Search for superresolution in a metamaterial solid immersion lens," *Phys. Rev. A*, vol. 99, 2019, Art. no. 023835.
[13] Z.-J. Yang, R. Jiang, X. Zhuo, Y.-M. Xie, J. Wang, and H.-Q. Lin, "Dielectric nanoresonators for light manipulation," *Phys. Rep.*, vol. 701, 2017, Art. no. 1.
[14] C. F. Kenworthy, L. Pjotr Stoevelaar, A. J. Alexander, and G. Gerini, "Using the near field optical trapping effect of a dielectric metasurface to improve SERS enhancement for virus detection," *Sci. Rep.*, vol. 11, 2021, Art. no. 6873.
[15] M. Iwanaga, "High-sensitivity high-throughput detection of nucleic acid targets on metasurface fluorescence biosensors," *Biosensors*, vol. 11, 2021, Art. no. 33.
[16] L. Ma *et al.*, "Thermally tunable high-Q metamaterial and sensing application based on liquid metals," *Opt. Exp.*, vol. 29, 2021, Art. no. 6069.
[17] L. Kang, H. Bao, and D. H. Werner, "Efficient second-harmonic generation in high Q-factor asymmetric lithium niobate metasurfaces," *Opt. Lett.*, vol. 46, 2021, Art. no. 633.
[18] J. C. Ginn *et al.*, "Realizing optical magnetism from dielectric metamaterials," *Phys. Rev. Lett.*, vol. 108, 2012, Art. no. 097402.
[19] S. Yang *et al.*, "Simultaneous excitation of extremely high-Q-factor trapped and octupolar modes in terahertz metamaterials," *Opt. Exp.*, vol. 25, 2017, Art. no. 15938.
[20] Y. Kivshar, "All-dielectric meta-optics and non-linear nanophotonics," *Nat. Sci. Rev.*, vol. 5, 2018, Art. no. 144.
[21] K. Koshelev, S. Lepeshov, M. Liu, A. Bogdanov, and Y. Kivshar, "Asymmetric metasurfaces with high-Q resonances governed by bound states in the continuum," *Phys. Rev. Lett.*, vol. 121, 2018, Art. no. 193903.
[22] Z. Sadrieva, K. Frizyuk, M. Petrov, Y. Kivshar, and A. Bogdanov, "Multipolar origin of bound states in the continuum," *Phys. Rev. B*, vol. 100, 2019, Art. no. 115303.
[23] S. Bakhti *et al.*, "Fano-like resonance emerging from magnetic and electric plasmon mode coupling in small arrays of gold particles," *Sci. Rep.*, vol. 6, 2016, Art. no. 32061.
[24] P. C. Wu *et al.*, "Optical anapole metamaterial," *ACS Nano*, vol. 12, 2018, Art. no. 1920.
[25] G.-D. Liu *et al.*, "A high-performance refractive index sensor based on Fano resonance in Si split-ring metasurface," *Plasmonics*, vol. 13, 2018, Art. no. 15.
[26] X. Chen and W. Fan, "Ultrahigh-Q toroidal dipole resonance in all-dielectric metamaterials for terahertz sensing," *Opt. Lett.*, vol. 44, 2019, Art. no. 5876.
[27] H. Liu *et al.*, "Metasurface generated polarization insensitive Fano resonance for high-performance refractive index sensing," *Opt. Exp.*, vol. 27, 2019, Art. no. 13252.
[28] K. E. Chong *et al.*, "Polarization-independent silicon metadevices for efficient optical wavefront control," *Nano Lett.*, vol. 15, 2015, Art. no. 5369.
[29] X. Liu, J. Li, Q. Zhang, and Y. Wang, "Dual-toroidal dipole excitation on permittivity-asymmetric dielectric metasurfaces," *Opt. Lett.*, vol. 45, 2020, Art. no. 2826.
[30] Y. Zhang *et al.*, "High-quality-factor multiple Fano resonances for refractive index sensing," *Opt. Lett.*, vol. 43, 2018, Art. no. 1842.
[31] S. Li, C. Zhou, T. Liu, and S. Xiao, "Symmetry-protected bound states in the continuum supported by all-dielectric metasurfaces," *Phys. Rev. A*, vol. 100, 2019, Art. no. 063803.
[32] C. Zhou, S. Li, Y. Wang, and M. Zhan, "Multiple toroidal dipole fano resonances of asymmetric dielectric nanohole arrays," *Phys. Rev. B*, vol. 100, 2019, Art. no. 195306.
[33] W. Wang, L. Zheng, L. Xiong, J. Qi, and B. Li, "High Q-factor multiple Fano resonances for high-sensitivity sensing in all-dielectric metamaterials," *OSA Continuum*, vol. 2, 2019, Art. no. 2818.
[34] W. Wang *et al.*, "Broken symmetry theta-shaped dielectric arrays for a high Q-factor Fano resonance with anapole excitation and magnetic field tunability," *OSA Continuum*, vol. 2, 2019, Art. no. 507.
[35] B. Ma *et al.*, "All-dielectric metasurface for sensing Microcystin-LR," *Electronics*, vol. 10, 2021, Art. no. 1363.
[36] H. Li, S. Yu, L. Yang, and T. Zhao, "High Q-factor multi-Fano resonances in all-dielectric double square hollow metamaterials," *Opt. Laser Technol.*, vol. 140, 2021, Art. no. 107072.